

Reducing Training Data Needs with Minimal Multilevel Machine Learning (M3L)

Stefan Heinen,¹ Danish Khan,^{1,2} Guido Falk von Rudorff,^{3,4} Konstantin Karandashev,⁵
Daniel Jose Arismendi Arrieta,⁶ Alastair J. A. Price,^{7,8} Surajit Nandi,⁹ Arghya
Bhowmik,⁹ Kersti Hermansson,⁶ and O. Anatole von Lilienfeld^{1, 7, 10, 11, 12, 13, *}

¹Vector Institute for Artificial Intelligence, Toronto, ON, M5S 1M1, Canada

²Department of Chemistry, University of Toronto, St. George Campus, Toronto, ON, Canada

³University Kassel, Department of Chemistry, Heinrich-Plett-Str.40, 34132 Kassel, Germany

⁴Center for Interdisciplinary Nanostructure Science and Technology (CINaT), Heinrich-Plett-Straße 40, 34132 Kassel

⁵University of Vienna, Faculty of Physics, Kolingasse 14-16, AT-1090 Wien, Austria

⁶Department of Chemistry-Ångström Laboratory, Uppsala University, Box 538, SE-75121 Uppsala, Sweden

⁷Acceleration Consortium, University of Toronto, 80 St George St, Toronto, ON M5S 3H6

⁸Departments of Chemistry, University of Toronto, St. George Campus, Toronto, ON, Canada

⁹Department of Energy Conversion and Storage, DTU, Anker Engelunds Vej, DK-2800 Kgs. Lyngby

¹⁰Department of Materials Science and Engineering,

University of Toronto, St. George campus, Toronto, ON, Canada

¹¹Department of Chemistry, University of Toronto, St. George campus, Toronto, ON, Canada

¹²Department of Physics, University of Toronto, St. George campus, Toronto, ON, Canada

¹³Machine Learning Group, Technische Universität Berlin and Berlin
Institute for the Foundations of Learning and Data, Berlin, Germany

For many machine learning applications in science, data acquisition, not training, is the bottleneck even when avoiding experiments and relying on computation and simulation. Correspondingly, and in order to reduce cost and carbon footprint, training data efficiency is key. We introduce minimal multilevel machine learning (M3L) which optimizes training data set sizes using a loss function at multiple levels of reference data in order to minimize a combination of prediction error with overall training data acquisition costs (as measured by computational wall-times). Numerical evidence has been obtained for calculated atomization energies and electron affinities of thousands of organic molecules at various levels of theory including HF, MP2, DLPNO-CCSD(T), DFHFCABS, PNOMP2F12, and PNOCCSD(T)F12, and treating tens with basis sets TZ, cc-pVTZ, and AVTZ-F12. Our M3L benchmarks for reaching chemical accuracy in distinct chemical compound sub-spaces indicate substantial computational cost reductions by factors of $\sim 1.01, 1.1, 3.8, 13.8$ and 25.8 when compared to heuristic sub-optimal multilevel machine learning (M2L) for the data sets QM7b, QM9^{LCCSD(T)}, EGP, QM9^{CCSD(T)}_{AE}, and QM9^{CCSD(T)}_{EA}, respectively. Furthermore, we use M2L to investigate the performance for 76 density functionals when used within multilevel learning and building on the following levels drawn from the hierarchy of Jacobs Ladder: LDA, GGA, mGGA, and hybrid functionals. Within M2L and the molecules considered, mGGAs do not provide any noticeable advantage over GGAs. Among the functionals considered and in combination with LDA, the three on average top performing GGA and Hybrid levels for atomization energies on QM9 using M3L correspond respectively to PW91, KT2, B97D, and τ -HCTH, B3LYP*(VWN5), TPSSH.

I. INTRODUCTION

Machine learning (ML) has revolutionized various scientific fields by leveraging large data sets to extract valuable insights. In 2012 Rupp *et al.* [1] introduced the first ML approach successfully learning atomization energies. However, the acquisition cost of training data remains a substantial bottleneck, often hindering progress in tackling new challenges. Even more so, data generation in general is still in its infancy: Most of all data has only been collected in the past two decades[2].

Additionally, we emphasize the significance of computational atomistic simulations, consuming approximately 35% of High-Performance Computing (HPC) budgets, which highlights the urgent need for more efficient

methodologies[3]. Recognizing the growing importance of sustainability, we also mention the environmental implications of using data-inefficient ML models; emphasizing the drive to make science greener. This latter point has become increasingly crucial in light of growing electricity prices. Hence, our research centers on minimizing training data acquisition cost and economizing data generation. Through the utilization of multilevel machine learning (M2L), we have refined the training set sizes using established legacy optimization techniques such as Bayesian optimization resulting in minimal multilevel machine learning (M3L). This strategic approach yields notable reduction in training acquisition time, all the while upholding model accuracy. Therefore, this work has the potential to greatly expedite the process of materials discovery by relieving the financial constraints linked to computational resources. The cost limitation, a frequent bottleneck for MAP optimizers, will be effectively eliminated through our proposed workflow.

* anatole.vonlilienfeld@utoronto.ca

Numerous researchers have already explored the realm of mitigating computational costs: Heinen *et al.*[3] in learning run times of quantum chemical (QC) calculations and using those predictions to optimize scheduling on super computers. Duan *et al.*[4] machine learned the success rate of transition metal geometry optimization calculations and therefore were able to stop potentially not converging calculations and free up space. Showing the importance of performance and cost in quantum chemistry and artificial intelligence (AI) for interatomic potentials is shown in Review[5]. This noteworthy review shows the impact of the computational discovery of materials in the era of big data[6]. Most recently, considerable amount of work has been invested in better algorithms such as central processing unit (GPU) enhanced density functional theory (DFT) codes[7, 8]. Furthermore, new improved representations like many body distribution functionals (MBDF)[9] among others[10–13] and new neural network infrastructures[14–17] minimizing the computational cost of either scaling linearly with system size or reducing the need for larger training data to achieve chemical accuracy (1kcal/mol). For the benchmark set QM9[18], modern representations in Kernel Ridge Regression (KRR) and Artificial Neural Networks (ANN) structure achieve chemical accuracy at 3000, 4000, 8000, 9000 training data for FCHL18[11], Allegro[17], FCHL19/PaiNN[12, 16], and SLATM[10], respectively. MBDF reaches Chemical accuracy at 10k, however, scaling linearly with size - therefore being compact - drastically reduces the training and prediction time[9]. A different approach is to pre-train a neural network on a lower level of theory and subsequently (using transfer learning) training the ANN on the higher level of theory, reducing the training cost[19–21]. Another noteworthy approach is to use a cheaper base line (Δ learning, Figure I a)) and predict the difference between the base line and the target level of theory. Already in 2015 multilevel learning was applied to protein-protein interactions using ANN[22]. Simultaneously, Ramakrishnan *et al.*[23] introduced Δ ML using a composite strategy that adds machine learning corrections to computationally inexpensive approximate legacy quantum methods to efficiently screen chemical compound space[24]. By adding a base line they were able to shift the learning curve to the left meaning a lower off set through adding a lower level of theory and therefore reducing the need for high level of theory training data. Most recently, Goodlett *et al.* compared different multi fidelity approaches for potential energy surface predictions[25], showing Δ learning as the most favorable approach. A drawback of this method is the need for a base line calculation on the lower level for each prediction. The main differences between Δ - and multilevel learning is that (a) the lowest level (base line) is learned not calculated, and (b) that one can benefit from having multiple levels of theory in the

data (as is shown in Figure I). Building upon previous work[26], we introduce Minimal Multilevel Machine Learning (M3L), we highlight the limitations of the previous heuristic-based multilevel machine learning (M2L) techniques, which lacked optimization.

M3L overcome this limitation by enhancing cost efficiency through systematic optimization of training set sizes at each level. To establish the efficacy of M3L, we have performed extensive numerical experimentation using datasets consisting of small organic molecules on various levels of theory, including Hartree-Fock (HF), MP2, Coupled Cluster Singles Doubles perturbative triples (CCSD(T)) on various basis sets (TZ, cc-pVTZ, and AVTZ-F12). We leverage Bayesian optimization to reduce the training set sizes required for higher levels of theory as shown in Figure I b1) and b2). Furthermore, we employ learning theory and learning curves[27] to make educated estimates of the training set sizes (Figure I b3). By applying these approaches, we successfully reduce the amount of high-level theory data needed while maintaining the desired accuracy. We provide numerical evidence showcasing the potential cost reductions offered by quantum mechanical data, highlighting their advantages compared to direct (conventional) quantum machine learning (QML), M2L and M3L approaches saving up to 25 times training data acquisition cost.

The algorithms proposed in this work can also be extended to evaluate the usefulness of intermediate steps of density functionals, the working horse in quantum machine learning[28], in Jacobs Ladder. We demonstrate that by considering 76 DFT functionals on Jacob’s ladder and showing that there are no discernible benefits of using mGGAs (meta-generalized gradient approximations) over GGAs (generalized gradient approximations) within this hierarchy.

II. METHODS

A. Kernel Ridge Regression

KRR[29, 30] was employed for all machine learning tasks using the QMLcode framework[31]. A detailed derivation can be found in Ref.[3]. To train a model, the regression coefficients α are calculated using the closed-form solution given by

$$\alpha = (\mathbf{K}^{\text{train}} + \lambda \mathbf{I})^{-1} \mathbf{y}^{\text{train}} \quad (1)$$

where $\mathbf{K}^{\text{train}}$ represents the training kernel, λ is the regularization strength which was not used in this work and \mathbf{I} is the identity matrix. Lambda is only necessary when there is numerical noise associated with the data or kernel inversion procedures for larger training set sizes or if there is considerable amount of noise present in the data. Since neither were a factor in this work we set it to zero.

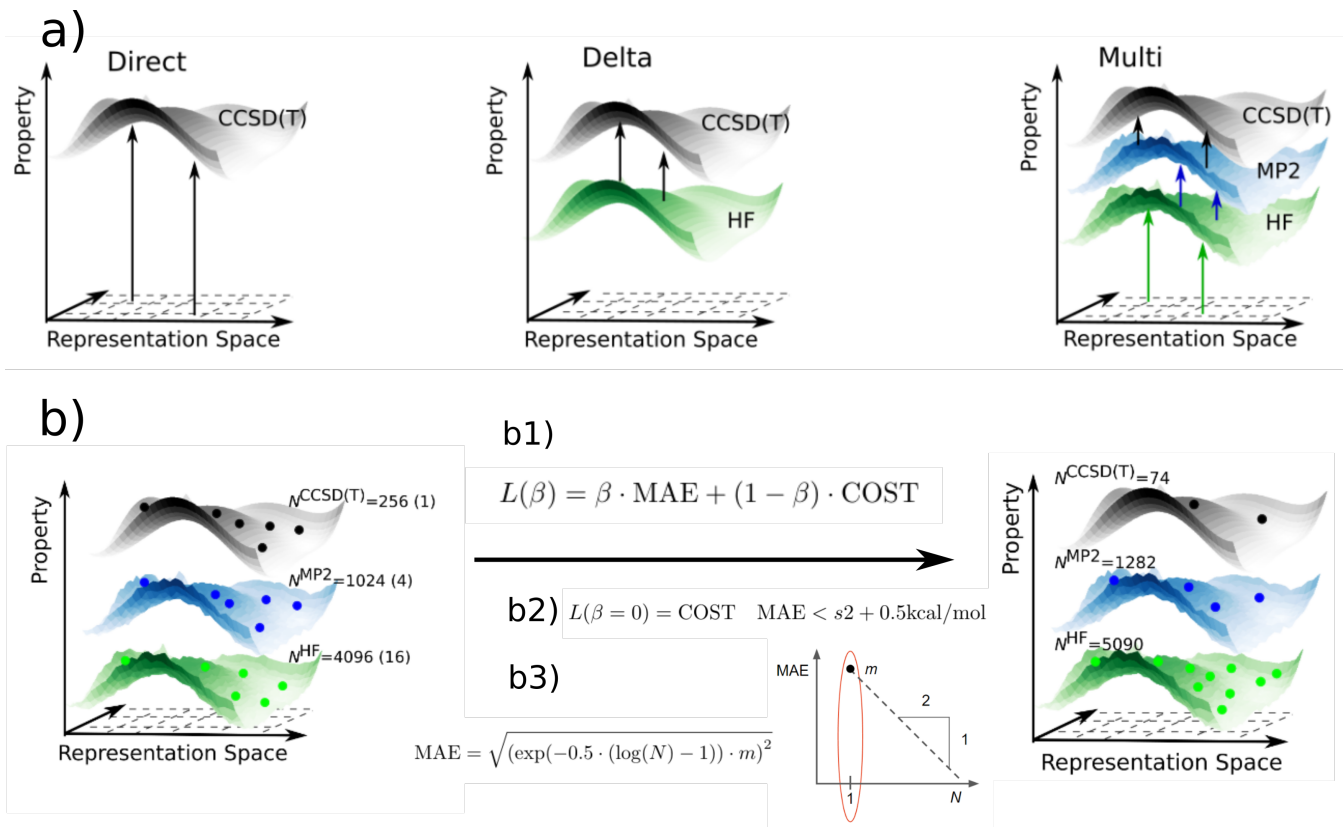


FIG. 1. (a) Fictitious potential energy surfaces for HF, MP2, and CCSD(T) showing the concept of direct, Δ , and multi-level learning, respectively. Arrows denote ML predictions, smooth surfaces calculated values (Back Surface target property (CCSD(T))) and coarse surfaces denote ML predictions. (b) Fictitious potential energy surfaces showing the training set sizes of the original work ($s2=1;4;16$) left and after Bayesian optimization (b1 and b2) with cost functions $L(\beta)$ and L with constraint $s2 < \text{MAE}$ or an educated guess using learning theory (b3) right, respectively. Using loss function in b2 for QM7b dataset yields new ratios right hand size on b) showing a reduction from 256 to 74 CCSD(T) training data.

For each Kernel element, a gaussian kernel was used

$$k(\mathbf{x}_i, \mathbf{x}_q) = \exp\left(-\frac{\|\mathbf{x}_i - \mathbf{x}_q\|_2^2}{2\sigma^2}\right), \quad (2)$$

where $k(\mathbf{x}_i, \mathbf{x}_q)$ is a Laplacian kernel element[32, 33]. To make ML based estimates y_q for a query compound \mathbf{x}_q , the following equation is used

$$y_q(\mathbf{x}_q) = \sum_i^N \alpha_i k(\mathbf{x}_i, \mathbf{x}_q). \quad (3)$$

Here, \mathbf{x} represents the representations, and σ is a hyperparameter. The hyperparameter σ was optimized using k -fold cross-validation, as described in[3]. The representation used throughout this work was MBDF from[9]. Since it is a compact presentation (scales linearly with system size), it allows for Bayesian optimizations by calling predictions multiple times for different training set sizes.

B. Multi-Level Learning

Zaspel *et al.* were the first to demonstrate the applicability of multilevel machine learning in terms of a grid-combination technique in 2018.[26]. Ratios between the different levels were chosen heuristically as $s1 = 2^0, 2^1, 2^2$ and $s2 = 2^0, 2^2, 2^4$ for the training set sizes $N^{\text{tot}} = N^{\text{CCSD(T)}} : N^{\text{MP2}} : N^{\text{HF}}$. The better performing ratios $s2$ from M2L were used in this work as a null model method to compare to. The ML based estimate of property y is as follows:

$$y_q^{\text{CCSD(T)}}(\mathbf{x}_q) = y_q^{\text{HF}}(\mathbf{x}_q) + y_q^{\text{HF} \rightarrow \text{MP2}}(\mathbf{x}_q) + y_q^{\text{MP2} \rightarrow \text{CCSD(T)}}(\mathbf{x}_q) \quad (4)$$

As shown in Figure I a) direct learning is performed for the lowest level ($y_q^{\text{HF}}(\mathbf{x}_q)$), while differences are learnt between the low-mid (HF \rightarrow MP2) and mid-high (MP2 \rightarrow CCSD(T)) levels. As evinced in that figure and as obvious from Eq. (3), the sum does not necessarily run over the same training molecules, implying that there is no need to obtain labels at all levels for any given training molecule.

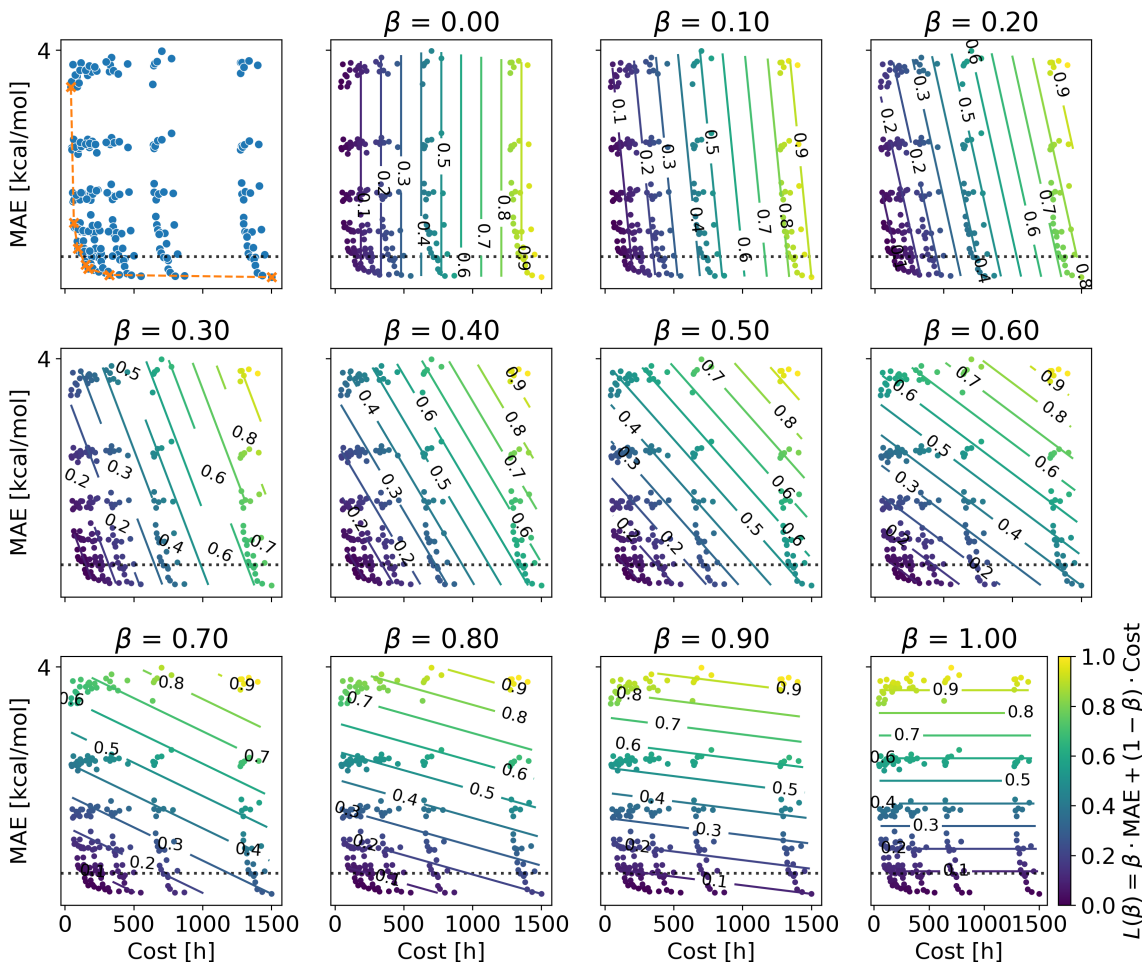


FIG. 2. Results of grid scan ($N_i = [175, 375, 750, 1500, 3000, 6000]$ for $i = \text{HF}, \text{MP2}, \text{CCSD(T)}$) shown for different values of β of cost function $L(\beta) = \beta \cdot \text{MAE}/\text{MAE}^{\max} + (1 - \beta) \cdot \text{Cost}/\text{Cost}^{\max}$ for the QM7b data set. Top left: Pareto front (orange) for the lowest values for $L(\beta)$ for each β

C. Data Sets

The following three datasets were used in this study:

- **QM7b**[34, 35]: This dataset includes 7,211 molecules with a maximum of 7 heavy atoms. The molecules contain elements such as C, N, O, S or Cl. Based on the string representation (SMILES[36, 37]) of molecules in the database, the universal force field[38] was used to generate reasonable 3D geometries, as implemented in OpenBabel[39]. The resulting geometries were relaxed using the PBE[40] level of theory and tier2 basis sets in the FHI-aims[41] electronic structure code.
- **QM9**[18, 42]: This dataset comprises 130k small organic molecules including C, N, O, F atoms. Geometries were optimized at the B3LYP/6-31G(2df,p)[43, 44] level of theory.

- **EGP**: The Electrolyte Genome Project (EGP)[45] contains ionization potential (IP) and electron affinities (EA) of 4830 molecules relevant to battery electrolytes at the B3LYP/6-31+G* level of theory.

which were divided into the five following subsets:

- **QM7b (toy set)**: On the QM7b DFT geometries Zaspel *et al.*[26] performed HF[46, 47], MP2[48, 49], and CCSD(T) Single Point calculations using three different basis sets (sto-3g[50, 51], 6-31G[52], cc-pVTZ[53]). cc-pVTZ was used in this work. The single point calculations were performed using Gaussian09[54].
- **QM9^{LCCSD(T)}**: For a subset of QM9 $\sim 18'000$ HF, MP2, and local PNO-LCCSD(T) calculations were performed on a cc-pVTZ basis set using ORCA5[55].

- **QM9^{CCSD(T)}_{AE/EA}**: This subset of the QM9 dataset includes atomization energies and electron affinities for $\sim 4'000$ molecules on PNO-CCSD(T)-F12/AVTZ-F12, and PNO-MP2/AVTZ-F12, DF-HF-CABS levels of theory, respectively. Electron affinities are composed of two calculation and the total run time of both was taken for this work. AE and EA stand for atomization energies and electron affinities, respectively. Another property in this data set are the ionization potentials. However, HF predictions are significantly worse compared to AE and EA, which makes learning inefficient. We excluded this data set from the main manuscript and put the learning curves in the SI.
- **EGP**: a subset was generated providing atomization energies containing 600 PNO-CCSDT-F12, 1'200 PNO-MP2, and 1'200 DF-HF-CABS levels of theory. The subset contains up to 15 heavy atoms (B, C, N, O, F, Si, P, S, Cl, and Br) 92 in total.
- **QM9^{DFT}**[56]: This dataset includes all 133k molecules in the QM9 dataset. For each molecule, atomization energies were calculated using 76 different functionals and three basis sets (SZ, DZ, TZ). The triple zeta basis set (TZ) was specifically used in this study.

D. Computational Cost & Loss Function

To combine both Mean Absolute Error (MAE) and CPU times (COST), a loss function ($L(\beta)$) was used. In this work, both properties were scaled between 0 and 1, and a weighted sum approach was employed:

$$L(\beta) = \beta \cdot \text{MAE} + (1 - \beta) \cdot \text{COST} \quad (5)$$

where $0 \leq \beta \leq 1$ represents the weight for MAE and the cost, respectively. The MAE is defined as:

$$\text{MAE} = \frac{\sum_q^N |y_{q,\text{est}} - y_{q,\text{ref}}|}{N} / \text{error}^{\text{max}} \quad (6)$$

and the COST is defined as:

$$\text{COST} = \frac{\left[\sum_i^{N^{\text{CCSD(T)}}} t_i^{\text{CCSD(T)}} + \sum_j^{N^{\text{MP2}}} t_j^{\text{MP2}} + \sum_k^{N^{\text{HF}}} t_k^{\text{HF}} \right]}{\text{COST}^{\text{max}}} \quad (7)$$

As the Gaussian electronic structure code[54] does not provide timing information, the approach described in[3] was used to predict CPU times for the calculations, estimating the cost of training set generation for the QM7b toy set. To predict the timings, the standard representation and KRR models were employed, substituting the property $\mathbf{y}^{\text{train}}$ with CPU times instead of atomization energies. For all other data sets, we obtained the

real/calculated timings from the output files, more details can be found in the SI. Figure 2 shows a grid scan for the QM7b data set for a range of training set sizes of $N_i = [175, 375, 750, 1500, 3000, 6000]$ for i being HF, MP2, CCSD(T), respectively. For every data point the loss function was evaluated for different values of β and color encoded in Figure 2. On the top left subplot the MAE were plotted in blue and the lowest value for each loss function was marked in orange, showing a Pareto front, indicating the validity of the weighted sum approach.

E. Bayesian Optimization

The Bayesian optimization as implemented in the scikit-optimize python library (skopt)[57] was used for optimizing the training set sizes in all datasets. This global integer optimization allowed for a broad scan of the training set sizes using: i) the loss function $L(\beta)$ (Eq. 5 and Figure I b1)) for different hyperparameters $\beta = [0.25, 0.5, 0.75]$, ii) using the same loss function but setting $\beta = 0$ giving $L(\beta = 0) = \text{COST}$ with the constraint of $\text{MAE} < s2$ described in Figure I b2).

F. Educated guess of training set size ratios

While the Bayesian optimization presented in this work reliably identifies the optimal weights between the different levels, it can be computationally expensive, even using a representation of constant size. A good initial guess for the weights can be obtained from learning curves[27, 29, 58]. It has been observed that direct learning curves exhibit a slope close to $-1/2$ for various representations and different tasks[9, 59]. Therefore, the MAE of direct learning approaches can be estimated from the null model, which represents the MAE when only one data point is given as shown in Figure I b3. The learning curve of multi-level learning can then be approximated by propagating the uncertainties of these individual models. In this case, direct learning of y_{HF} is combined with learning the differences between HF and MP2, as well as the differences between MP2 and CCSD. The total cost C in this model depends on the number of training points N for different methods of average cost c :

$$C = N_{\text{HF}} \cdot c_{\text{HF}} + N_{\text{MP2}} \cdot c_{\text{MP2}} + N_{\text{CCSD}} \cdot c_{\text{CCSD}} \quad (8)$$

Meanwhile, the MAE M in the multi-level approach is estimated to emerge from the null model accuracies m_l , where l stands for HF, MP2, and CCSD(T), respectively and can be derived as follows using the *Ansatz* in Figure

I b3:

$$\log(\text{MAE}) = -\frac{1}{2}N + \log(m) - \frac{1}{2} \quad (9)$$

$$= -\frac{1}{2}(N-1) + \log(m) \quad (10)$$

$$\text{MAE} = \exp\left(-\frac{1}{2}(N-1) + \log(m)\right) \quad (11)$$

$$= m \cdot \exp\left(-\frac{1}{2}(N-1)\right) \quad (12)$$

using equation 12 and error propagation for all three levels l leads to the final equation:

$$\text{MAE} = \sqrt{\sum_{l \in \{\text{HF}, \text{MP2}, \text{CCSD}\}} (\exp(-0.5 \cdot (\log(N_l) - 1)) \cdot m_l)^2} \quad (13)$$

Following short code example was used to get the optimal ratio using an average COST estimate C and the null model error m_l :

```
import numpy as np
import itertools as it

c = {"HF": 0.016, "MP": 0.039, "CC": 0.235}
ml = {"HF": 35.7, "MP": 6.16, "CC": 2.76}

def cost_and_error(N_HF, N_MP, N_CC):
    c = N_HF*c["HF"]+N_MP*c["MP"]+N_CC*c["CC"]
    eA = ml["HF"]*np.exp(-0.5*(np.log(N_HF)-1))
    eB = ml["MP"]*np.exp(-0.5*(np.log(N_MP)-1))
    eC = ml["CC"]*np.exp(-0.5*(np.log(N_CC)-1))
    return cost, np.sqrt(eA**2+eB**2+eC**2)

def optimal_for_error(thres):
    lvl = [int(_) for _ in 2**np.linspace(0,15)]

    mcost = 1e100
    opt = None
    for NHF,NMP,NCC in it.product(lvl,lvl,lvl):
        cost,error = cost_and_error(NHF,NMP,NCC)
        if cost < mcost and error < thres:
            mcost = cost
            opt = (NHF, NMP, NCC)
    return opt
```

III. RESULTS AND DISCUSSION

A. Minimizing Training Acquisition Cost within M3L

We optimized the training set ratios at different levels of theory (CCSD(T):MP2:HF) using Bayesian optimization with $N^{\text{CCSD(T)}}$, N^{MP2} , and N^{HF} as parameters. We utilized the s2 ratio as initial points for both loss functions $L(\beta)$ (equation 5) for $\beta = [0.25, 0.5, 0.75]$, and we also employed the constraint loss function $L(\beta = 0) = \text{COST}$ (Figure I b2). Additionally, we obtained ratios using the "fancy guess" approach leveraging learning theory and the optimal behaviour of learning curves with a slope of $-1/2$.

TABLE I. Summary of all subsets reporting ratios of CCSD(T) equal to 1, MP2, HF, total number of highest level training data ($N^{\text{CCSD(T)}}$) where each model reaches chemical accuracy (1kcal/mol) and the total CPU time in h needed (CPU^{tot}) to train those models. Green cells report best models (lowest training acquisition time). Yellow cells report models where the learning curve could not be extrapolated correctly due to optimizer reach too small training data of the highest levels of theory.

	Subsets	MP2	HF	$N^{\text{CCSD(T)}}$	CPU^{tot} [h]
QM7b	Guess	7	68	101	150.2
	M2L	4	16	232	151.6
	$\beta=0$ (constr.)	17	67	74	150.7
	$\beta=0.25$	104	514	107	1358
	$\beta=0.50$	235	917	47	1159
	$\beta=0.75$	3	17	243	149
QM9 ^{LCCSD(T)}	Guess	3	35	962	6398
	M2L	4	16	1333	6941
	$\beta=0$ (constr.)	10	39	813	7127
	$\beta=0.25$	20	100	290	7690
	$\beta=0.50$	5	36	643	6346
	$\beta=0.75$	10	23	1018	8436
QM9 ^{CCSD(T)} _{AE}	Guess	6	162	594	1337
	M2L	4	16	2508	3227
	$\beta=0$ (constr.)	47	187	413	2061
	$\beta=0.25$	30	411	77	400
	$\beta=0.50$	13	160	418	1130
	$\beta=0.75$	10	221	302	853
QM9 ^{CCSD(T)} _{EA}	Guess	2	23	18763	12871
	M2L	4	16	75163	128077
	$\beta=0$ (constr.)	10	35	1921	4951
	$\beta=0.25$	8	252	1866	9387
	$\beta=0.50$	58	290	684	7550
	$\beta=0.75$	16	49	1987	7128
EGP	Guess	20	150	370	1951
	M2L	4	16	6787	10382
	$\beta=0$ (constr.)	6	20	3529	7601
	$\beta=0.25$	8	80	455	1535
	$\beta=0.50$	5	36	917	1921
	$\beta=0.75$	13	65	268	751

To evaluate the models, we generated learning curves showing the mean absolute error (MAE) vs. the training set size of the highest level of theory ($N^{\text{CCSD(T)}}$). Figure 3 presents learning curves for all subsets. Notably, all models showed improved performance with increasing training set sizes, with CCSD(T) being the highest level, MP2 the intermediate level, and HF the lowest level of theory. Direct learning exhibited the worst performance, while the heuristic model s2 performed slightly better but was outperformed by the optimized models.

Table I summarizes the results for all subsets, reporting the ratios MP2 and HF w.r.t CCSD(T) equal to 1, as well as the number of training data for CCSD(T) ($N^{\text{CCSD(T)}}$) and the total CPU time required for training data acquisition time (CPU^{tot}). The models with the lowest training acquisition time are highlighted in green, while models with suboptimal learning curves due to limited training data for the highest level are marked in red. Those

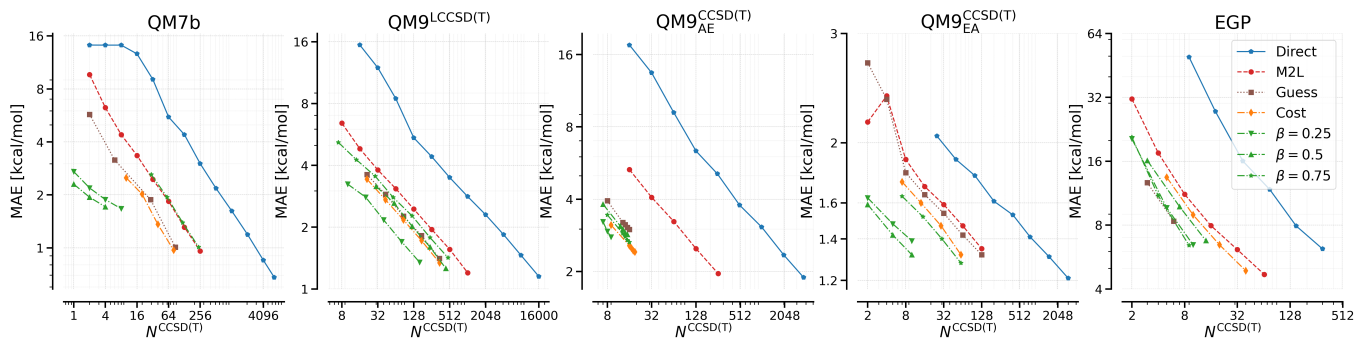


FIG. 3. Learning curves showing MAE vs. $N^{\text{CCSD(T)}}$ (highest level of theory) for each subset for direct learning, original work (M2L), educated guess (Guess), Bayesian optimizations (Cost ($\beta = 0$) and different β 's), respectively.

being for QM7b the models $\beta = 0.25$ and 0.5 with high ratios of MP2 and HF with 1:104:514 for $\beta = 0.25$ and 1:235:917 for $\beta = 0.5$, respectively. In the small training data range of 1 to 8 training points (Figure 3) smaller slopes were observed, limiting the slope of the learning curves. Adding more training data will lead to a similar slopes compared to the other learning curves. For the subset $\text{QM9}_{\text{AE}}^{\text{CCSD(T)}}$ the learning curve for $\beta = 0.25$ has to be analyzed with caution. Similarly, to QM7b learning curves discussed above, the low data range may not represent the real slope of the learning curve, which again, will converge to the slope of the other learning curves. Excluding those learning curves, the best models for all subsets are $\beta = 0.75$, $\beta = 0.5$, $\beta = 0.75$, $\beta = 0$ (constr.), and $\beta = 0.75$ for QM7b, $\text{QM9}^{\text{LCCSD(T)}}$, $\text{QM9}^{\text{CCSD(T)}}$, $\text{QM9}^{\text{LCCSD(T)}}$, $\text{QM9}_{\text{EA}}^{\text{CCSD(T)}}$, and EGP, respectively. It is evident that the Bayesian optimization models consistently outperformed other approaches using high β values, achieving a reduction in training set size of the highest level and significantly reducing training acquisition time compared to the original work *s2*. The "fancy guess" approach yielded promising results in a fraction of the time needed by the Bayesian optimization, giving a good first and cheap estimate of optimal ratios.

To further evaluate the models, critical points for each dataset were analyzed, displaying the training set size of the highest level of theory vs. the total cost (CPU hours) at 1kcal/mol (extrapolated through a linear fit using the slope of the learning curves). The original work *s2* was used as a reference point (black circles around points in Figure 4). Models that show fewer training data needed for smaller datasets (QM7b and $\text{QM9}^{\text{LCCSD(T)}}$) and faster/less accurate calculations are considered more efficient, even though no significant gain in cost was achieved. On the other hand, for larger datasets like EGP and the electron affinities for QM9, a reduction in the need for high-level training data and significant time savings were observed. The models marked in yellow in Table I with limited training data for the highest level are expected to perform worse due to the inaccurate extrapolation of learning curves. However, with more data, the models' performance is likely to improve, and the total

training acquisition time would be further reduced.

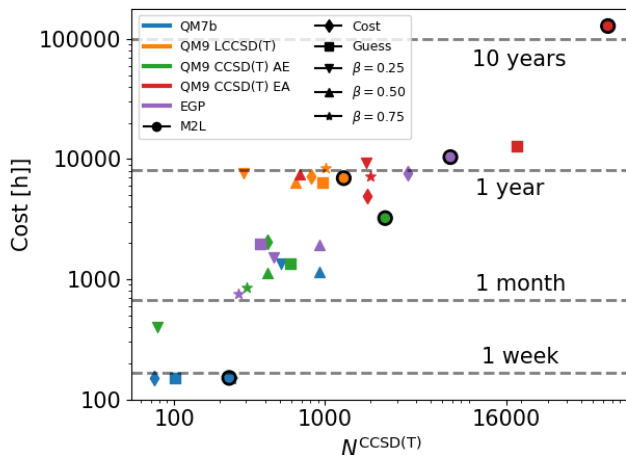


FIG. 4. Critical points of chemical accuracy on the Pareto front of total training acquisition time vs. training data of the highest level of theory ($N^{\text{CCSD(T)}}$) for all datasets (QM7b, QM9 LCCSD(T), QM9 CCSD(T) atomization energies and electron affinities, and EGP) where each model reaches chemical accuracy (1 kcal/mol) extrapolated from corresponding learning curves. Original work (M2L) encircled in black.

B. Density Functional Approximations within M2L

Density Functional Theory has emerged as a powerful computational tool for studying a wide range of chemical systems due to its advantageous trade-off between efficiency and accuracy. Key to the success of DFT are the various functionals, each designed with distinct focuses and approximations. Among these, Generalized Gradient Approximations (GGAs) stand out, leveraging the reduced density gradient to achieve semi-local behavior. However, GGAs fall short in capturing critical physical aspects, leading to the development of meta-GGAs that aim to include additional quantities like τ and $\nabla^2\rho$.

Although several meta-GGAs exist, many rely heavily on empirical approaches, resulting in marginal improvements over GGA functionals.

To attain superior accuracy over GGAs, hybrid functionals have proven to be highly effective. The global hybrid functional takes the form of $E_{X\sigma}^{\text{hybrid}} = aE_{X\sigma}^{\text{HF}} + (1-a)E_{X\sigma}^{\text{GGA}}$, where the precise value of 'a' typically falls in the range of 20-50%, depending on the functional. In the realm of Chemistry, hybrid functionals outperform both pure HF and GGA functionals, providing valuable insights into various chemical problems.

However, the use of hybrid functionals necessitates parametrization. The widely-used B3LYP functional, for instance, contains three parameters represented as $E_{\text{XC}} = aE_{X\sigma}^{\text{HF}} + (1-a)E_{X\sigma}^{\text{LSDA}} + b\delta E_{X\sigma}^{\text{GGA}} + E_{\text{C}}^{\text{LSDA}} + c\delta E_{\text{C}}^{\text{GGA}}$. While parametrization can enhance performance to some extent, it comes with potential drawbacks, including deleterious effects on numerical sensitivity and oscillatory behavior in the enhancement factor containing the reduced density gradient. Over-fitting issues, as observed in the Minnesota functionals, also arise in the parametrization process.

Another critical aspect of density functionals is the absence of dispersion characterization in base functionals, impacting the modeling of intermolecular interactions. To address this, post-SCF corrections are commonly employed, such as D3 corrections [60] being a widely used and accurate approach.

Since there are so many density functionals, with different flavours and parametrizations[61], we investigated the hierarchy of Jacob's ladder for the QM9^{DFT} dataset containing single-point calculations for 76 functionals per molecule, and using the original M2L ratio *s2* to train several machine learning models. Figure 5 presents the MAE for all combinations of LDA→GGA→Hybrid (left) and LDA→mGGA→Hybrid (right) for the atomization energies. The rows and columns in the in Figure 5 are sorted according to the mean errors of each model, providing insights into the performance of different functionals at each level of theory.

Despite the diversity of density functionals, the results showed that there was no significant gain in using mGGA over GGA, considering the higher calculation timings without any clear benefit. Notably, some functionals, such as PBE-D and VS98-X(XC), performed poorly overall in both GGA and mGGA cases. This could be attributed to the missing dispersion correction in most hybrid functionals for PBE-D. On the other hand, B97-D, KT2, and PW91 emerged as the best performing functionals for the GGA case, while BECKE00, TPSS-D, and TPSS were the top performers for the mGGA case.

Interestingly, B3LYP flavors consistently reached the top three positions among the hybrid functionals for both GGA and mGGA cases. In contrast, KMLYP and BHANDH flavors underperformed in both cases, rendering them unsuitable for multi-level learning approaches. Furthermore, combining B97 with the best-performing hybrid functionals yielded the lowest errors in the GGA

case.

In conclusion, density functionals exhibit varying performance levels, and the combination of different datasets to lift a target dataset onto a higher level of theory could be a viable approach in real-world applications. Although mGGA functionals did not provide significant advantages over GGA functionals, multi-level learning with different steps on Jacob's ladder remains feasible, especially considering the widespread use of density functional theory in machine learning applications.

Overall, our findings demonstrate the potential for significant reductions in training acquisition cost using Bayesian optimization and the efficacy of multi-level learning with density functional theory in quantum chemistry applications.

IV. CONCLUSION

In this study, we introduced M3L as a means to minimize training acquisition cost for machine learning models in quantum chemistry applications. Through Bayesian optimization, we optimized the ratios of quantum chemistry levels (CCSD(T):MP2:HF) to achieve the most efficient learning curves. Our M3L results demonstrate the effectiveness of this approach in reducing the training set size of the highest level of theory and significantly reduce training acquisition costs by up to 18 times compared to the original heuristic M2L approach (*s2*).

The Bayesian optimization models consistently outperformed other approaches, providing better ratios and resulting in more efficient learning curves. Moreover, the Educated Guess approach showed promise, achieving similar performance to the Bayesian optimization models but with a fraction of the cost. However, further exploration and comparison on larger datasets are warranted to fully evaluate its potential.

Additionally, we investigated the hierarchy of Jacob's ladder for density functional theory (DFT) using the QM9^{DFT} dataset. Surprisingly, we found no significant advantage in using meta-GGA (mGGA) functionals over generalized gradient approximation (GGA) functionals, despite the higher complexity (including more physics) for mGGA. This suggests that for multi-level learning with DFT, GGA functionals might be more efficient without compromising accuracy. Furthermore, we identified the best-performing functionals for both GGA and mGGA cases, highlighting the importance of choosing suitable functionals for specific applications.

V. SUPPLEMENTARY INFORMATION

All data, scripts, and results will be comprehensively documented within the final publication. Should there be a need, interested parties are welcome to request these materials directly from the authors.

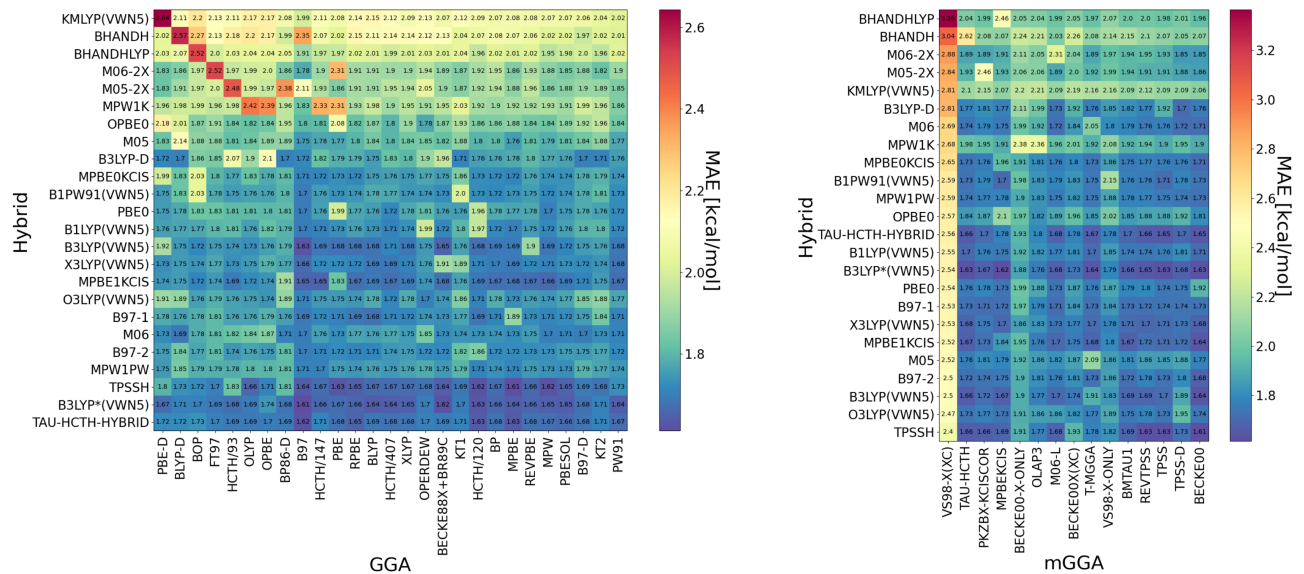


FIG. 5. MAE for all combinations of LDA→GGA→Hybrid (left) and LDA→mGGA→Hybrid (right) for QM9 dataset. Rows and columns are sorted according to the mean errors of each column and row, showing no advantage of mGGAs over GGAs in multi-level learning.

ACKNOWLEDGEMENT

The author of this manuscript utilized Chat-GPT3.5. They assume complete responsibility for every sentence presented in the document. O.A.v.L. has received funding from the European Research Council (ERC) under the European Union’s Horizon 2020 research and innovation programme (grant agreement No. 772834). This project has received funding from the European Union’s Horizon 2020 research and innovation programme under grant agreement No. 957189. This research was

undertaken thanks in part to funding provided to the University of Toronto’s Acceleration Consortium from the Canada First Research Excellence Fund (CFREF). O.A.v.L. has received support as the Ed Clark Chair of Advanced Materials and as a Canada CIFAR AI Chair. This result only reflects the author’s view and the EU is not responsible for any use that may be made of the information it contains. The project has been supported by the Swedish Research Council (Vetenskapsrådet), and the project the prothe Swedish National Strategic e-Science program eSENCE as well as by computing resources from the Swedish National Infrastructure for Computing (SNIC/NAISS).

- [1] M. Rupp, A. Tkatchenko, K.-R. Müller, and O. A. von Lilienfeld, Fast and accurate modeling of molecular atomization energies with machine learning, *Physical Review Letters* **108**, 10.1103/physrevlett.108.058301 (2012).
- [2] O. Y. Al-Jarrah, P. D. Yoo, S. Muhaidat, G. K. Karagiannidis, and K. Taha, Efficient machine learning for big data: A review, *Big Data Research* **2**, 87 (2015).
- [3] S. Heinen, M. Schwilk, G. F. von Rudorff, and O. A. von Lilienfeld, Machine learning the computational cost of quantum chemistry, *Machine Learning: Science and Technology* **1**, 025002 (2020).
- [4] C. Duan, J. P. Janet, F. Liu, A. Nandy, and H. J. Kulik, Learning from failure: Predicting electronic structure calculation outcomes with machine learning models, *Journal of Chemical Theory and Computation* **15**, 2331 (2019).
- [5] Y. Zuo, C. Chen, X. Li, Z. Deng, Y. Chen, J. Behler, G. Csányi, A. V. Shapeev, A. P. Thompson, M. A. Wood, and S. P. Ong, Performance and cost assessment of machine learning interatomic potentials, *The Journal of Physical Chemistry A* **124**, 731 (2020).
- [6] Z. Lu, Computational discovery of energy materials in the era of big data and machine learning: A critical review, *Materials Reports: Energy* **1**, 100047 (2021).
- [7] E. Epifanovsky, A. T. Gilbert, X. Feng, J. Lee, Y. Mao, N. Mardirossian, P. Pokhilko, A. F. White, M. P. Coons, A. L. Dempwolff, *et al.*, Software for the frontiers of quantum chemistry: An overview of developments in the q-chem 5 package, *The Journal of chemical physics* **155** (2021).
- [8] X. Andrade, C. D. Pemmaraju, A. Kartsev, J. Xiao, A. Lindenberg, S. Rajpurohit, L. Z. Tan, T. Ogitsu, and A. A. Correa, Inq, a modern GPU-accelerated computational framework for (time-dependent) density functional theory, *Journal of Chemical Theory and Computation* **17**, 7447 (2021).

- [9] D. Khan, S. Heinen, and O. A. von Lilienfeld, Kernel based quantum machine learning at record rate : Many-body distribution functionals as compact representations (2023).
- [10] B. Huang and O. A. von Lilienfeld, Quantum machine learning using atom-in-molecule-based fragments selected on the fly, *Nature Chemistry* **12**, 945 (2020).
- [11] F. A. Faber, A. S. Christensen, B. Huang, and O. A. von Lilienfeld, Alchemical and structural distribution based representation for universal quantum machine learning, *The Journal of Chemical Physics* **148**, 241717 (2018), <https://doi.org/10.1063/1.5020710>.
- [12] A. S. Christensen, L. A. Bratholm, F. A. Faber, and O. Anatole von Lilienfeld, Fchl revisited: Faster and more accurate quantum machine learning, *The Journal of Chemical Physics* **152**, 044107 (2020), <https://doi.org/10.1063/1.5126701>.
- [13] M. J. Willatt, F. Musil, and M. Ceriotti, Feature optimization for atomistic machine learning yields a data-driven construction of the periodic table of the elements, *Phys. Chem. Chem. Phys.* **20**, 29661 (2018).
- [14] K. T. Schütt, P. Kessel, M. Gastegger, K. A. Nicoli, A. Tkatchenko, and K.-R. Müller, SchNetPack: A deep learning toolbox for atomistic systems, *Journal of Chemical Theory and Computation* **15**, 448 (2018).
- [15] K. Schütt, P.-J. Kindermans, H. E. Sauceda Felix, S. Chmiela, A. Tkatchenko, and K.-R. Müller, Schnet: A continuous-filter convolutional neural network for modeling quantum interactions, in *Advances in Neural Information Processing Systems*, Vol. 30, edited by I. Guyon, U. V. Luxburg, S. Bengio, H. Wallach, R. Fergus, S. Vishwanathan, and R. Garnett (Curran Associates, Inc., 2017).
- [16] K. T. Schütt, O. T. Unke, and M. Gastegger, Equivariant message passing for the prediction of tensorial properties and molecular spectra, *CoRR* **abs/2102.03150** (2021), 2102.03150.
- [17] A. Musaelian, S. Batzner, A. Johansson, L. Sun, C. J. Owen, M. Kornbluth, and B. Kozinsky, Learning local equivariant representations for large-scale atomistic dynamics, *Nature Communications* **14**, 10.1038/s41467-023-36329-y (2023).
- [18] R. Ramakrishnan, P. O. Dral, M. Rupp, and O. A. von Lilienfeld, Quantum chemistry structures and properties of 134 kilo molecules, *Scientific Data* **1** (2014).
- [19] D. Jha, K. Choudhary, F. Tavazza, W. keng Liao, A. Choudhary, C. Campbell, and A. Agrawal, Enhancing materials property prediction by leveraging computational and experimental data using deep transfer learning, *Nature Communications* **10**, 10.1038/s41467-019-13297-w (2019).
- [20] H. Yamada, C. Liu, S. Wu, Y. Koyama, S. Ju, J. Shiomi, J. Morikawa, and R. Yoshida, Predicting materials properties with little data using shotgun transfer learning, *ACS Central Science* **5**, 1717 (2019).
- [21] N. J. Lentelink and S. Palkovits, Transfer learning as tool to enhance predictions of molecular properties based on 2d projections, *Advanced Theory and Simulations* **3**, 2000148 (2020).
- [22] J. Zubek, M. Tatjewski, A. Boniecki, M. Mnich, S. Basu, and D. Plewczynski, Multi-level machine learning prediction of protein protein interactions in *saccharomyces cerevisiae*, *PeerJ* **3**, e1041 (2015).
- [23] R. Ramakrishnan, P. O. Dral, M. Rupp, and O. A. von Lilienfeld, Big data meets quantum chemistry approximations: The delta-machine learning approach, *Journal of Chemical Theory and Computation* **11**, 2087 (2015).
- [24] O. A. von Lilienfeld, K.-R. Müller, and A. Tkatchenko, Exploring chemical compound space with quantum-based machine learning, *Nature Reviews Chemistry* **4**, 347 (2020).
- [25] S. M. Goodlett, J. M. Turney, and H. F. Schaefer, Comparison of multifidelity machine learning models for potential energy surfaces, *The Journal of Chemical Physics* **159**, 10.1063/5.0158919 (2023).
- [26] P. Zaspel, B. Huang, H. Harbrecht, and O. A. von Lilienfeld, Boosting quantum machine learning models with a multilevel combination technique: Pople diagrams revisited, *Journal of Chemical Theory and Computation* **15**, 1546 (2018).
- [27] C. Cortes, L. D. Jackel, S. A. Solla, V. Vapnik, and J. S. Denker, Learning curves: Asymptotic values and rate of convergence, in *Advances in Neural Information Processing Systems* (1994) pp. 327–334.
- [28] B. Huang, G. F. von Rudorff, and O. A. von Lilienfeld, The central role of density functional theory in the AI age, *Science* **381**, 170 (2023).
- [29] V. N. Vapnik, *Statistical Learning Theory* (Wiley-Interscience, 1998).
- [30] C. E. Rasmussen and C. K. I. Williams, *Gaussian processes for machine learning.*, Adaptive computation and machine learning (MIT Press, 2006) pp. I–XVIII, 1–248.
- [31] A. S. Christensen, F. A. Faber, B. Huang, L. A. Bratholm, A. Tkatchenko, K.-R. Müller, and O. A. von Lilienfeld, Qml: A python toolkit for quantum machine learning, <https://github.com/qmlcode/qml> (2017).
- [32] M. P. Deisenroth, A. A. Faisal, and C. S. Ong, *Mathematics for Machine Learning* (Cambridge University Press, 2020).
- [33] K. T. Schütt, S. Chmiela, O. A. von Lilienfeld, A. Tkatchenko, K. Tsuda, and K.-R. Müller, *Machine Learning Meets Quantum Physics* (Springer, 2020).
- [34] G. Montavon, M. Rupp, V. Gobre, A. Vazquez-Mayagoitia, K. Hansen, A. Tkatchenko, K.-R. Müller, and O. A. von Lilienfeld, Machine learning of molecular electronic properties in chemical compound space, *New Journal of Physics* **15**, 095003 (2013).
- [35] L. C. Blum and J.-L. Reymond, 970 million druglike small molecules for virtual screening in the chemical universe database GDB-13, *J. Am. Chem. Soc.* **131**, 8732 (2009).
- [36] D. Weininger, SMILES, a chemical language and information system. 1. introduction to methodology and encoding rules, *Journal of Chemical Information and Computer Sciences* **28**, 31 (1988).
- [37] D. Weininger, SMILES. 3. DEPICT. graphical depiction of chemical structures, *Journal of Chemical Information and Computer Sciences* **30**, 237 (1990).
- [38] A. K. Rappé, C. J. Casewit, K. S. Colwell, W. A. G. III, and W. M. Skid, Uff, a full periodic table force field for molecular mechanics and molecular dynamics simulations, *J. Am. Chem. Soc.* **114**, 10024 (1992).
- [39] N. M. O'Boyle, M. Banck, C. A. James, C. Morley, T. Vandermeersch, and G. R. Hutchison, Open babel: An open chemical toolbox, *Journal of Cheminformatics* **3**, 10.1186/1758-2946-3-33 (2011).

- [40] J. P. Perdew, K. Burke, and M. Ernzerhof, Generalized gradient approximation made simple, *Physical Review Letters* **77**, 3865 (1996).
- [41] V. Blum, M. Rossi, S. Kokott, and M. Scheffler, The fhi-aims code: All-electron, ab initio materials simulations towards the exascale (2022).
- [42] L. Ruddigkeit, R. van Deursen, L. C. Blum, and J.-L. Reymond, Enumeration of 166 billion organic small molecules in the chemical universe database GDB-17, *Journal of Chemical Information and Modeling* **52**, 2864 (2012).
- [43] A. D. Becke, Density-functional thermochemistry. iii. the role of exact exchange, *J. Chem. Phys* **98**, 5648 (1993).
- [44] C. Lee, W. Yang, and R. G. Parr, Development of the colle-salvetti correlation-energy formula into a functional of the electron density, *Phys. Rev. B* **37**, 785 (1988).
- [45] X. Qu, A. Jain, N. N. Rajput, L. Cheng, Y. Zhang, S. P. Ong, M. Brafman, E. Maginn, L. A. Curtiss, and K. A. Persson, The electrolyte genome project: A big data approach in battery materials discovery, *Comput. Mater. Sci.* **103**, 56 (2015).
- [46] D. R. Hartree, The wave mechanics of an atom with a non-coulomb central field. part II. some results and discussion, *Mathematical Proceedings of the Cambridge Philosophical Society* **24**, 111 (1928).
- [47] J. C. Slater, The self consistent field and the structure of atoms, *Physical Review* **32**, 339 (1928).
- [48] M. J. Frisch, M. Head-Gordon, and J. A. Pople, A direct MP2 gradient method, *Chemical Physics Letters* **166**, 275 (1990).
- [49] M. Head-Gordon, J. A. Pople, and M. J. Frisch, MP2 energy evaluation by direct methods, *Chemical Physics Letters* **153**, 503 (1988).
- [50] W. J. Hehre, R. F. Stewart, and J. A. Pople, Self-consistent molecular-orbital methods. i. use of gaussian expansions of slater-type atomic orbitals, *The Journal of Chemical Physics* **51**, 2657 (1969).
- [51] J. B. Collins, P. von R. Schleyer, J. S. Binkley, and J. A. Pople, Self-consistent molecular orbital methods. XVII. geometries and binding energies of second-row molecules. a comparison of three basis sets, *The Journal of Chemical Physics* **64**, 5142 (1976).
- [52] R. Ditchfield, W. J. Hehre, and J. A. Pople, Self-consistent molecular-orbital methods. IX. an extended gaussian-type basis for molecular-orbital studies of organic molecules, *The Journal of Chemical Physics* **54**, 724 (1971).
- [53] R. A. Kendall, T. H. Dunning, and R. J. Harrison, Electron affinities of the first-row atoms revisited. systematic basis sets and wave functions, *The Journal of Chemical Physics* **96**, 6796 (1992).
- [54] M. J. Frisch, G. W. Trucks, H. B. Schlegel, G. E. Scuseria, M. A. Robb, J. R. Cheeseman, G. Scalmani, V. Barone, B. Mennucci, G. A. Petersson, H. Nakatsuji, M. Caricato, X. Li, H. P. Hratchian, A. F. Izmaylov, J. Bloino, G. Zheng, J. L. Sonnenberg, M. Hada, M. Ehara, K. Toyota, R. Fukuda, J. Hasegawa, M. Ishida, T. Nakajima, Y. Honda, O. Kitao, H. Nakai, T. Vreven, J. A. Montgomery, Jr., J. E. Peralta, F. Ogliaro, M. Bearpark, J. J. Heyd, E. Brothers, K. N. Kudin, V. N. Staroverov, R. Kobayashi, J. Normand, K. Raghavachari, A. Rendell, J. C. Burant, S. S. Iyengar, J. Tomasi, M. Cossi, N. Rega, J. M. Millam, M. Klene, J. E. Knox, J. B. Cross, V. Bakken, C. Adamo, J. Jaramillo, R. Gomperts, R. E. Stratmann, O. Yazyev, A. J. Austin, R. Cammi, C. Pomelli, J. W. Ochterski, R. L. Martin, K. Morokuma, V. G. Zakrzewski, G. A. Voth, P. Salvador, J. J. Dannenberg, S. Dapprich, A. D. Daniels, O. Farkas, J. B. Foresman, J. V. Ortiz, J. Cioslowski, and D. J. Fox, *Gaussian 09 Revision E.01* (2009), gaussian Inc. Wallingford CT 2009.
- [55] F. Neese, Software update: The orca program system version 5.0, *WIREs Computational Molecular Science* **12**, 10.1002/wcms.1606 (2022).
- [56] S. Nandi, T. Vegge, and A. Bhowmik, Large dataset of molecular and reaction energies from multi-level quantum chemical methods (2022).
- [57] F. Pedregosa, G. Varoquaux, A. Gramfort, V. Michel, B. Thirion, O. Grisel, M. Blondel, P. Prettenhofer, R. Weiss, V. Dubourg, J. Vanderplas, A. Passos, D. Cournapeau, M. Brucher, M. Perrot, and E. Duchesnay, Scikit-learn: Machine learning in Python, *Journal of Machine Learning Research* **12**, 2825 (2011).
- [58] K. R. Müller, M. Finke, N. Murata, K. Schulten, and S. Amari, A numerical study on learning curves in stochastic multilayer feedforward networks, *Nuovo Cimento* **8**, 1085 (1996).
- [59] F. A. Faber, L. Hutchison, B. Huang, J. Gilmer, S. S. Schoenholz, G. E. Dahl, O. Vinyals, S. Kearnes, P. F. Riley, and O. A. von Lilienfeld, Prediction errors of molecular machine learning models lower than hybrid dft error, *Journal of Chemical Theory and Computation* **13**, 5255 (2017), pMID: 28926232, <https://doi.org/10.1021/acs.jctc.7b00577>.
- [60] L. Goerigk, A comprehensive overview of the DFT-d3 london-dispersion correction, in *Non-Covalent Interactions in Quantum Chemistry and Physics* (Elsevier, 2017) pp. 195–219.
- [61] L. Goerigk, A. Hansen, C. Bauer, S. Ehrlich, A. Najibi, and S. Grimme, A look at the density functional theory zoo with the advanced GMTKN55 database for general main group thermochemistry, kinetics and noncovalent interactions, *Physical Chemistry Chemical Physics* **19**, 32184 (2017).